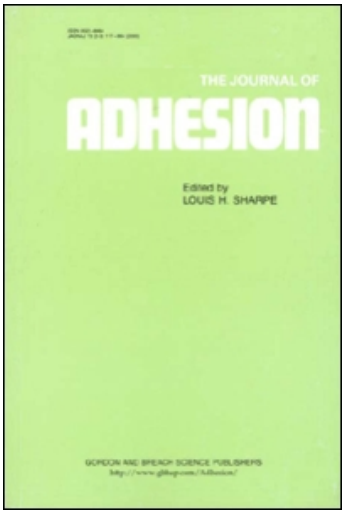

The Journal of Adhesion
Publication details, including instructions for authors and subscription information:
http://www.informaworld.com/smpp/title~content=t713453635

Effect of Adhesive Type and Thickness on the Lap Shear Strength

Lucas F. M. da Silva[a]; T. N. S. S. Rodrigues[a]; M. A. V. Figueiredo[a]; M. F. S. F. de Moura[a]; J. A. G. Chousal[a]
[a] Department of Mechanical Engineering and Industrial Management, Faculty of Engineering, University of Porto, Portugal

To cite this Article Silva, Lucas F. M. da , Rodrigues, T. N. S. S. , Figueiredo, M. A. V. , de Moura, M. F. S. F. and Chousal, J. A. G.(2006) 'Effect of Adhesive Type and Thickness on the Lap Shear Strength', The Journal of Adhesion, 82: 11, 1091 — 1115
To link to this Article: DOI: 10.1080/00218460600948511
URL: http://dx.doi.org/10.1080/00218460600948511

The Journal of Adhesion, 82:1091–1115, 2006

ISSN: 0021-8464 print/1545-5823 online
DOI: 10.1080/00218460600948511

Taylor & Francis
Taylor & Francis Group

Effect of Adhesive Type and Thickness on the Lap Shear Strength

Lucas F. M. da Silva
T. N. S. S. Rodrigues
M. A. V. Figueiredo
M. F. S. F. de Moura
J. A. G. Chousal
Department of Mechanical Engineering and Industrial Management, Faculty of Engineering of the University of Porto, Portugal

The effect of the adhesive thickness on the bond strength of single-lap adhesive joints is still not perfectly understood. The classical elastic analyses predict that the strength increases with the adhesive thickness, whereas experimental results show the opposite. Various theories have been proposed to explain this discrepancy, but more experimental tests are necessary to understand all the variables.

The objective of the present study was to assess the effect of the adhesive thickness on the strength of single-lap joints for different kinds of adhesives. Three different adhesives were selected and tested in bulk. The strain to failure in tension ranged from 1.3% for the most brittle adhesive to 44% for the most ductile adhesive. The adherend selected was a high-strength steel to keep the adherends in the elastic range and simplify the analysis. Three thicknesses were studied for each adhesive: 0.2, 0.5, and 1 mm.

A statistical analysis of the experimental results shows that the lap shear strength increases as the bondline gets thinner and the adhesive gets tougher.

Keywords: Adhesive thickness; Epoxy; Finite element analysis; Lap shear strength; Mechanical properties of adhesives; Statistical analysis

Received 21 January 2006; in final form 13 July 2006.

Address correspondence to Lucas F. M. da Silva, Departamento de Engenharia Mecânica e Gestão Industrial, Faculdade de Engenharia da Universidade do Porto, Rua Dr. Roberto Frias, 4200-465 Porto, Portugal. E-mail: lucas@fe.up.pt

1. INTRODUCTION

The effect of adhesive thickness on the strength of adhesively bonded joints still needs investigation. Practice shows that the lap-joint strength increases as the bondline gets thinner. The highest strength is obtained for bondlines on the order of 0.05 to 0.5 mm. However, this broad observation is not applicable to all cases as there are other variables involved, such as the type of loading (shear, peel, or cleavage), the adherend behaviour (elastic or plastic), and the type of adhesive (ductile or brittle). For example, for peel joints and ductile adhesives, the failure load increases as the bondline gets thicker because the adhesive is able to distribute the load over a larger area [1]. In the case of adhesive joints used for the determination of fracture energy such as the double cantilever beam or the compact tension, the effect of bondline thickness varies. Lee *et al.* [2] state that as the bondline thickness decreases, the fracture energy either decreases monotonically or increases, peaks, and then decreases rapidly depending on the adhesive ductility and crack path.

The single-lap joint is the most common type of joint, and it is important to quantify the effect of the adhesive thickness for design purposes. The classical analytical analyses such as those of Volkersen [3] or Goland and Reissner [4] are not in accordance with the available experimental results. Other authors have proposed other theories.

Crocombe [5] shows that thicker single-lap joints have a lower strength considering the plasticity of the adhesive. An elastic analysis shows that the stress distribution of a thin bondline is more concentrated at the ends of the overlap than a thicker bondline, which has a more uniform stress distribution. Therefore, a thin bondline will reach the yielding stress at a lower load than a thick bondline. However, when yielding does occur in a thicker joint, there is a less "elastic reserve" to sustain further loading, and thus, yielding spreads more quickly.

Another theory to explain the effect of the adhesive thickness on the strength of single-lap joints was introduced by Gleich *et al.* in 2001 [6]. They show with a finite element analysis that the interface stresses (peel and shear) increase as the bondline gets thicker. Supposing that the failure occurs close to the adhesive–adherend interface, a failure criterion based on the interface stresses can explain why thin joints are stronger than thick joints.

Another earlier theory proposed by Adams and Peppiatt [7] explains the discrepancy by saying that thicker bondlines contain more defects such as voids and microcracks. The theoretical and experimental results available in the literature are for typical structural adhesives with intermediate properties and do not consider the case of an

extremely brittle adhesive and the case of a very ductile adhesive. It is well known that a single-lap joint experiences high peel loading at the ends of the overlap in addition to shear loading. The joint strength is a function of the adhesive strength and ability to distribute the load over a large area and reduce the stress concentration.

In the present work, we investigated the type of adhesive that leads to the highest load-bearing capacity in a single-lap joint and how the joint strength is affected by the adhesive thickness. Three types of adhesives (brittle, intermediate, and ductile) were selected based on information from suppliers. The adhesives were then tested in bulk to confirm the mechanical properties. Single-lap joints were manufactured and tested according to a plan based on the Taguchi method [8], and the experimental results were statistically treated to determine the influence of the type of adhesive and the adhesive thickness. A finite element analysis was also carried out to simulate the lap shear tests for a better theoretical understanding.

2. EXPERIMENTAL

Three adhesives were selected: a very ductile adhesive (Hysol EA 9361 from Loctite, Munich, Germany), a very brittle adhesive (Araldite AV138/HV998 from Huntsman, Salt Lake City, UT, USA), and an intermediate adhesive (Hysol EA 9321 from Loctite). According to Crocombe's proposition [5], a joint with a ductile adhesive should give a strength that increases with a decrease of the bondline thickness while a brittle adhesive with no plasticity should give a strength that increases with the adhesive thickness.

The technique described in the French standard NF T 76-142 [9,10] for producing plate specimens without porosity was used. Two-millimetre-thick plate specimens of the three adhesives were manufactured in a sealed mould, and dogbone specimens were machined from those plates afterwards. The geometry of the dogbone specimens is presented in Fig. 1. The specimens were tensile tested in a MTS machine (MTS, Eden Prairie, MN, USA) under a crosshead speed of 1 mm/min. Three specimens were tested for each adhesive. The strain was measured using a specially designed noncontacting technique for objects suffering high displacement fields, as in tensile tests, developed by Chousal and Gomes [11]. Contacting extensometers tend to interfere with the mechanical behaviour of the adhesive [12] and should be avoided when possible. The technique used here is an optical method in which the displacements/strains are obtained by spatial correlation of image pairs acquired initially (nondeformed) and through loading. The loading images were acquired at regular

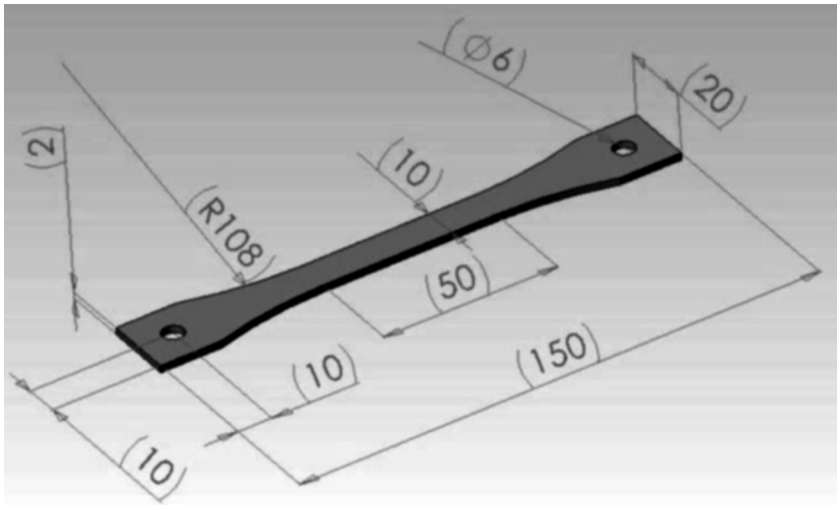

FIGURE 1 Dogbone specimen for tensile testing (dimensions in mm).

intervals (generally every 5 s) from which an in-house computer programme calculated the corresponding displacements/strains. The camera had a resolution of 8 megapixels, and the images were taken with an infrared remote control, ensuring the camera stability (see Fig. 2). One of the advantages of this technique is its ability to measure displacements without the need of specimen surface marks, because the texture of the surface (speckle-like) is generally sufficient for displacement tracking.

Typical stress–strain curves of the adhesives are shown in Fig. 3. The mechanical properties of the adhesives used are shown in Table 1. The brittle adhesive, AV138/HV998, presents more scatter than the other adhesives because it is more sensitive to defects. However, the failure surface did not contain any noticeable voids. The yield strength was calculated for a plastic deformation of 0.2%. The area under the stress–strain curve (U_T) is an approximate value of the toughness [13]:

$$\begin{aligned} U_T &= \left(\frac{\sigma_{ya} + \sigma_r}{2}\right)\varepsilon_f \quad \text{(ductile)} \\ U_T &= \frac{2}{3}\sigma_r\varepsilon_f \quad \text{(brittle)} \end{aligned} \tag{1}$$

where σ_{ya} is the yield strength of the adhesive, σ_r is the ultimate tensile strength, and ε_f is the failure strain. To quantify separately the influence of the adhesive thickness and the type of adhesive (toughness, U_T) on the lap shear strength, the experimental design technique of

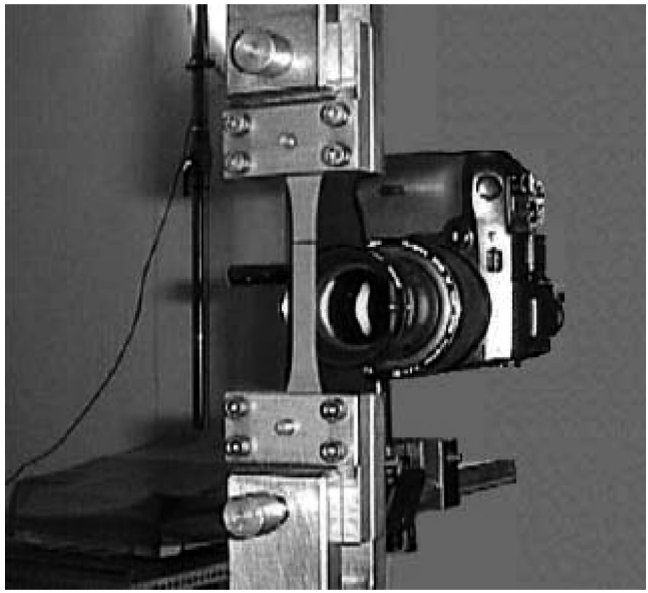

FIGURE 2 Measurement of the tensile deformation by an optical method.

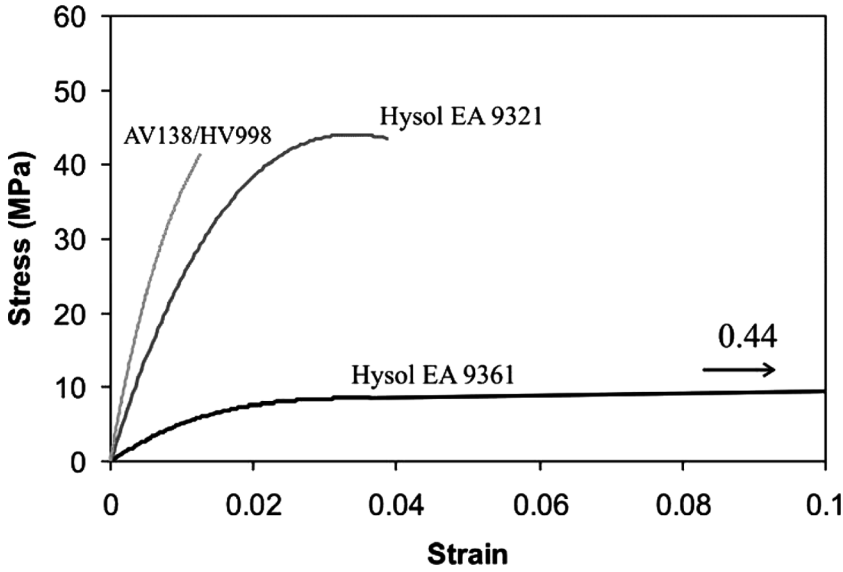

FIGURE 3 Tensile stress–strain curves of the various adhesives tested.

TABLE 1 Adhesive Properties (Three Specimens Tested for Each Temperature)

Parameter	Hysol EA 9361	Hysol EA 9321	AV138/HV998
Young's modulus E (GPa)	0.67 ± 0.02	3.87 ± 0.15	4.59 ± 0.81
Poisson's ratio[a] ν	0.4	0.36	0.35
Yield strength σ_{ya} (MPa)	4.23 ± 0.55	21.99 ± 2.16	36.49 ± 2.47
Tensile strength σ_r (MPa)	7.99 ± 1.59	45.97 ± 0.09	41.01 ± 7.28
Failure strain ε_f (%)	44.0 ± 12.3	3.8 ± 0.03	1.3 ± 0.44
Toughness U_T (MPa)	2.69	1.16	0.34

[a]Manufacturer's data.

Taguchi [14] was used. An experimental orthogonal array (L_9) of three levels with nine experimental runs was designed. After assigning the variables (type of adhesive and adhesive thickness) to the columns of the L_9 matrix and the respective values for each level, the experimental plan presented in Table 2 was obtained and repeated six times. The influence of each variable and the interactions among them was assessed by the average response and the analysis of variance (ANOVA). The statistical software Statview (SAS Institute, Inc., Cary, NC, USA) was used.

The single-lap joints (SLJs) had an overlap of 25 mm and a width of 25 mm (see geometry in Fig. 4). To maintain the adherends in the elastic range, a high-strength steel was chosen (DIN C60, quenched in oil). The overlap length was chosen according to a simple methodology proposed by Adams and Davies [15]. The load corresponding to the total plastic deformation of the adhesive is

$$F_a = \tau_y \cdot w \cdot l, \tag{2}$$

TABLE 2 Experimental Plan Based on Taguchi Orthogonal Array (L_9)

Experimental run	Type of adhesive	Adhesive thickness (mm)
1	AV138	0.2
2	AV138	0.5
3	AV138	1
4	EA 9321	0.2
5	EA 9321	0.5
6	EA 9321	1
7	EA 9361	0.2
8	EA 9361	0.5
9	EA 9361	1

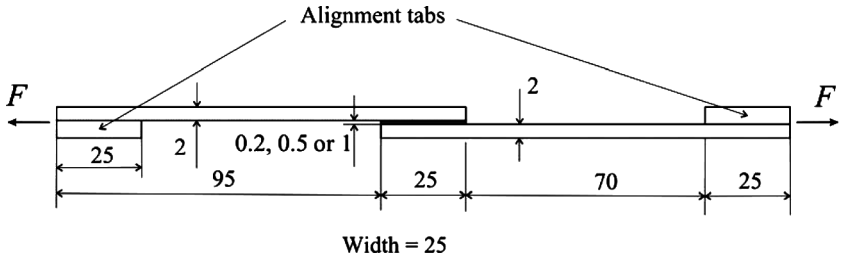

FIGURE 4 Single-lap joints geometry (not to scale, dimensions in mm).

where F_a is the failure load of the adhesive, τ_y is the yield strength of the adhesive, w is the joint width, and l is the overlap length. The direct tensile stress (σ_t) acting in the adherend due to the applied load F is

$$\sigma_t = \frac{F}{wt_s}, \tag{3}$$

where t_s is the adherend thickness. The stress at the inner adherend surface (σ_s) due to the bending moment M is

$$\sigma_s = \frac{6M}{wt_s^2}, \tag{4}$$

where $M = kFt_s/2$, according to Goland and Reissner [4]. The variable k is the bending moment factor, which reduces (from unity) as the lap rotates under load. The stress acting in the adherend is the sum of the direct stress and the bending stress. Thus, the maximum load that can be carried that just creates adherend yield (F_s) is

$$F_s = \frac{\sigma_{ys} wt_s}{1 + 3k}, \tag{5}$$

where σ_{ys} is the yield strength of the adherend. For low loads and short overlaps, k is approximately 1. Therefore, for such a case,

$$F_s = \frac{\sigma_{ys} wt_s}{4}. \tag{6}$$

However, for joints that are long compared to the adherend thickness, such that $l/t_s \geq 20$, the value of k decreases and tends to zero. In this case, the whole of the cross-section yields and

$$F_s = \sigma_{ys} \cdot w \cdot t_s. \tag{7}$$

The adherend will not yield if $F_s > F_a$. This condition (considering the adhesive that has the higher shear strength) means that the

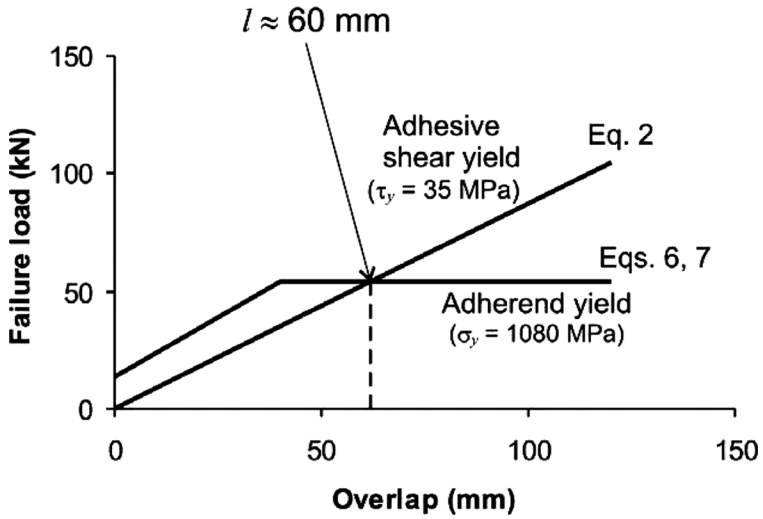

FIGURE 5 Methodology to predict the overlap corresponding to adherend yield.

overlap length (l) must be lower than approximately 60 mm, as shown in Fig. 5.

The SLJs were manufactured individually in a mould, and the adhesive thickness (0.2, 0.5, and 1 mm) was controlled by packing shims. The steel substrates were grit blasted and degreased prior to bonding. The tensile shear tests were performed in the same machine as the adhesive dogbone specimens at a crosshead speed of 1 mm/min. Tab ends were used to improve alignment, as shown in Fig. 4.

3. LAP SHEAR STRENGTH RESULTS

The experimental failure loads of the SLJs are shown in Fig. 6. The failed joints all had a cohesive failure, but very close to the interface, as shown in Fig. 7. As expected, the joint strength of the ductile adhesive (Hysol EA 9361) decreases as the bondline gets thicker, in accordance with Crocombe's [5] theory. This is also true for the intermediate adhesive (Hysol EA 9321). For the brittle adhesive (AV138/HV998), the joint strength increases from 0.2 to 0.5 and decreases from 0.5 to 1 mm. However, this trend should be analysed with caution because if one looks at the scatter (Figs. 8, 9, and 10), the increase from 0.2 to 0.5 mm for the brittle adhesive (AV138/HV998) HV998) presents an important dispersion. This is because brittle adhesives are very sensitive to defects such as voids and microcracks. Anyway, from 0.5 to 1 mm, there is definitely a decrease in the SLJ

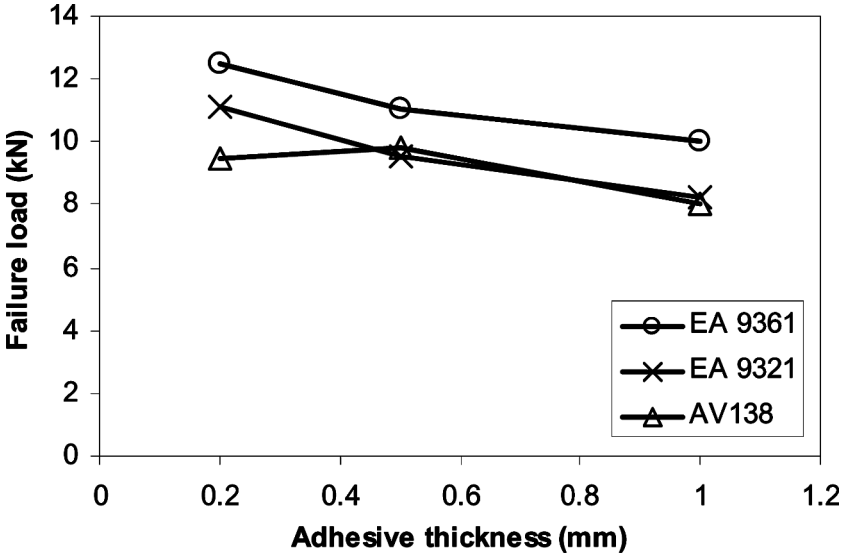

FIGURE 6 SLJs' failure load as a function of adhesive type and thickness.

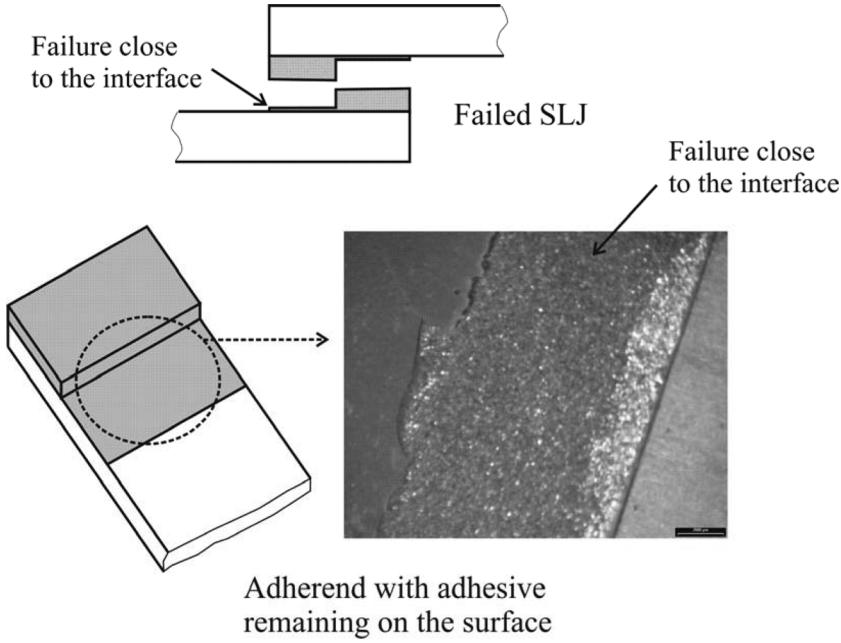

FIGURE 7 Fracture surface of a SLJ.

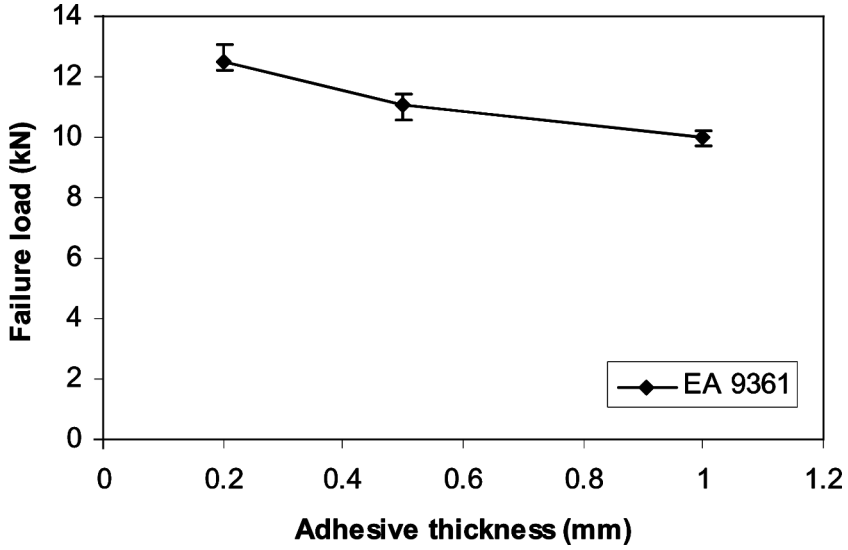

FIGURE 8 Scatter in adhesive Hysol EA 9361 SLJs' failure load.

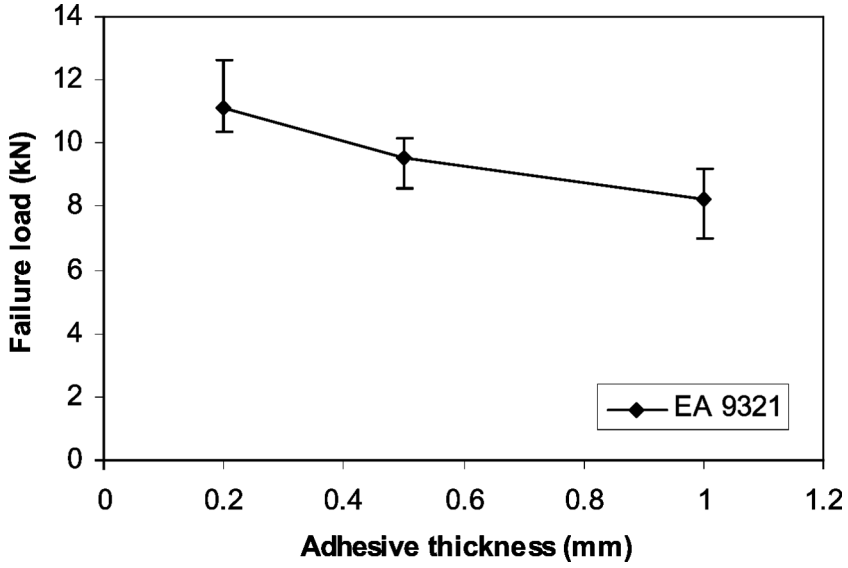

FIGURE 9 Scatter in adhesive Hysol EA 9321 SLJs' failure load.

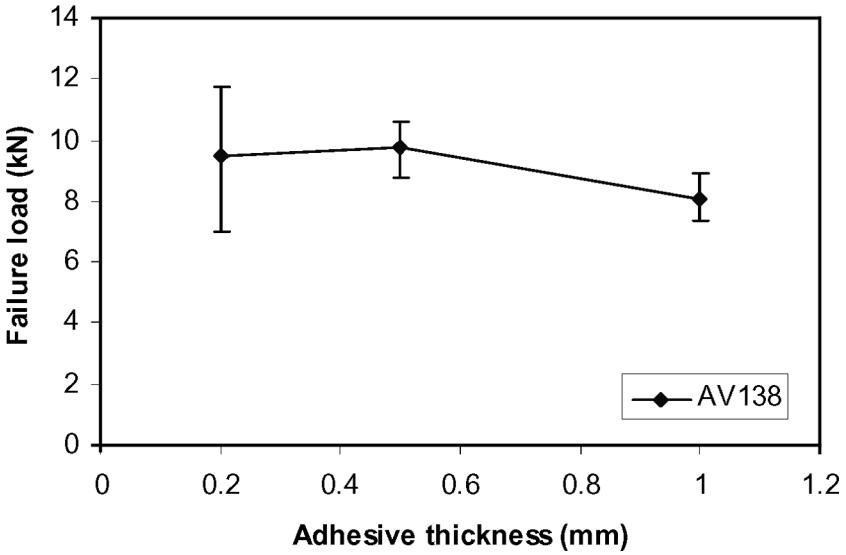

FIGURE 10 Scatter in adhesive AV138/HV998 SLJs' failure load.

strength, and this is not in accordance with an elastic prediction, which should be applicable when the adhesive is very brittle and has practically no plastic deformation. Therefore, the joint strength cannot be solely explained by the plastic behaviour of the adhesive.

Other important experimental data to analyse are the load-displacements curves. The curves for the intermediate and brittle adhesives are very similar (Figs. 11 and 12), because in both cases the adhesive deformation is negligible in comparison with that of the steel. However, the curves for the ductile adhesive contain two regions (see Fig. 13). The second region with a lower slope is probably due to the plastic deformation of the adhesive, but this would mean that the joint with a thinner bondline started to deform plastically at a higher load than the thicker joints, which is in disagreement with a plastic finite element analysis. Note also that the slope decreases as the bondline increases, which means that the joint is becoming more flexible.

4. FINITE ELEMENT ANALYSIS

4.1. Details

A finite element analysis of the SLJs was carried out to explain the experimental results. A two-dimensional (2D) plane-strain model

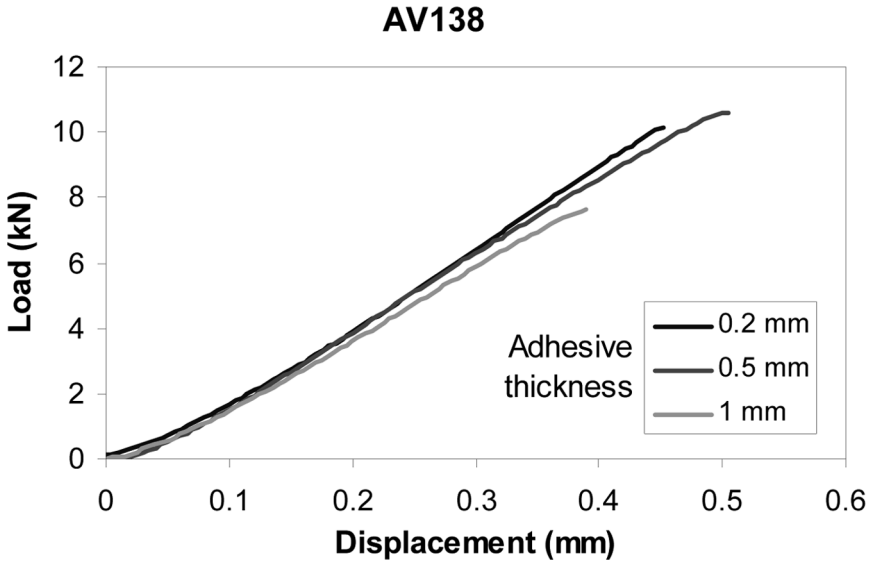

FIGURE 11 Load-displacement curves for the brittle adhesive AV138/HV998.

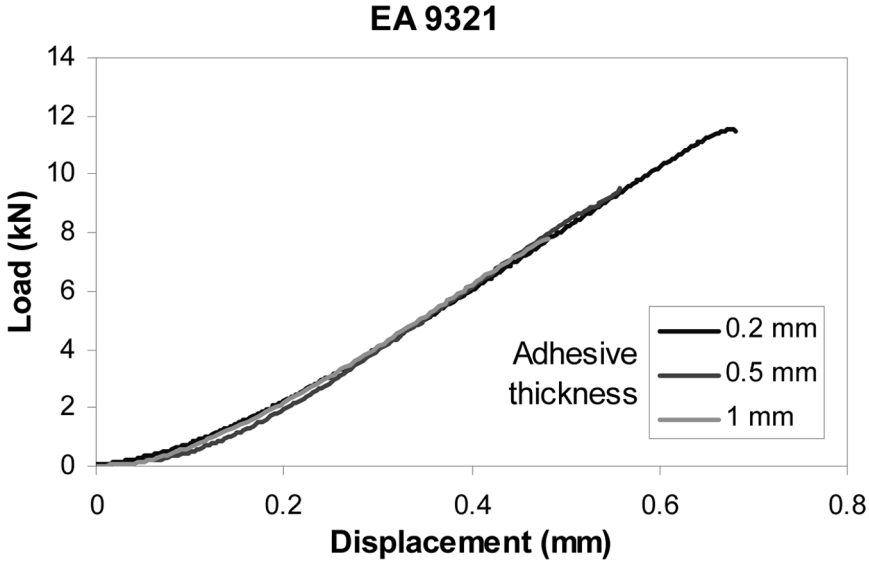

FIGURE 12 Load-displacement curves for the intermediate adhesive Hysol EA 9321.

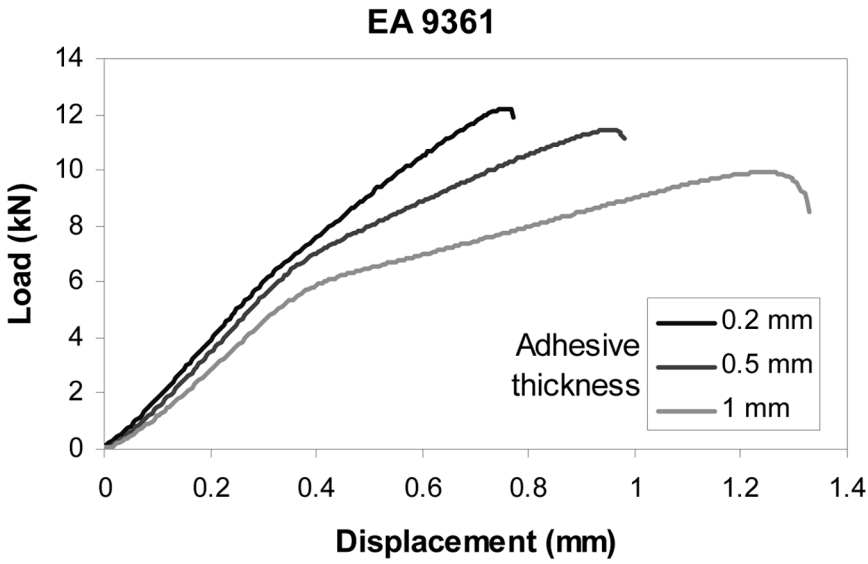

FIGURE 13 Experimental load-displacement curves for the ductile adhesive Hysol EA 9361.

was used. Interface finite elements including a progressive damage model were also considered. The six-node interface finite element for 2D problems is compatible with the eight-node plane solid elements and was implemented into the ABAQUS® commercial code as a user subroutine. The formulation was based on a constitutive relationship between stresses and relative displacements. Before damage started to grow, the stresses at the interface finite element were calculated from

$$\boldsymbol{\sigma} = \mathbf{D}\boldsymbol{\delta}, \tag{8}$$

where $\boldsymbol{\delta}$ is the vector of relative displacements between homologous points of the element and $\mathbf{D}$ a diagonal matrix containing the interface stiffnesses introduced by the user [16,17]. When the material strength $\sigma_{u,i}$ is attained (the subscript i is the mode of loading, which can be mode I or mode II), a softening process between stresses and interfacial relative displacements occurs. In this work, $\sigma_{u,i}$ was assumed to be equal to the yielding strength of the adhesive. Failure was assumed to take place progressively as energy dissipated gradually at the crack tip. The softening stress/relative displacement is

$$\boldsymbol{\sigma} = (\mathbf{I} - \mathbf{E})\mathbf{D}\boldsymbol{\delta}, \tag{9}$$

where **I** is the identity matrix and **E** a diagonal matrix containing the damage parameters defined by

$$e_i = \frac{\delta_{u,i}(\delta_i - \delta_{o,i})}{\delta_i(\delta_{u,i} - \delta_{o,i})}, \tag{10}$$

where δ_i is the current relative displacement in mode i and $\delta_{o,i}$ the displacement corresponding to the onset of damage. In pure mode loading, the strength along other directions is abruptly cancelled. The maximum relative displacement $\delta_{u,i}$, for which complete failure occurs, was obtained by equating the area under the softening curve to the respective critical fracture energy

$$G_{ic} = \frac{1}{2}\sigma_{u,i}\delta_{u,i}. \tag{11}$$

In adhesive joints, a complex stress state is present, and damage propagation occurs under mixed-mode loading (mode I and II). Therefore, a formulation for interface elements should include a mixed-mode damage model, which, in this case, is an extension of the pure mode model described previously. Damage initiation was predicted by using a quadratic stress criterion

$$\begin{aligned} &\left(\frac{\sigma_{\mathrm{I}}}{\sigma_{u,\mathrm{I}}}\right)^2 + \left(\frac{\sigma_{\mathrm{II}}}{\sigma_{u,\mathrm{II}}}\right)^2 = 1 \qquad && \text{if } \sigma_{\mathrm{I}} \geq 0, \\ &\sigma_{\mathrm{II}} = \sigma_{u,\mathrm{II}} && \text{if } \sigma_{\mathrm{I}} \leq 0, \end{aligned} \tag{12}$$

with the assumption that normal compressive stresses do not promote damage. For damage propagation a linear energetic criterion was considered:

$$\frac{G_{\mathrm{I}}}{G_{\mathrm{Ic}}} + \frac{G_{\mathrm{II}}}{G_{\mathrm{IIc}}} = 1. \tag{13}$$

The released energy in each mode at complete failure can be obtained from the area of the minor triangle of Fig. 14:

$$G_i = \frac{1}{2}\sigma_{um,i}\delta_{um,i}. \tag{14}$$

From the relationships between stresses and relative displacements [Eq. (8)] and from the relationship between released energies and relative displacements [Eqs. (14) and (11)], the problem can be implemented as a function of relative displacements. The relative displacements for each mode corresponding to damage onset, $\delta_{om,i}$, and

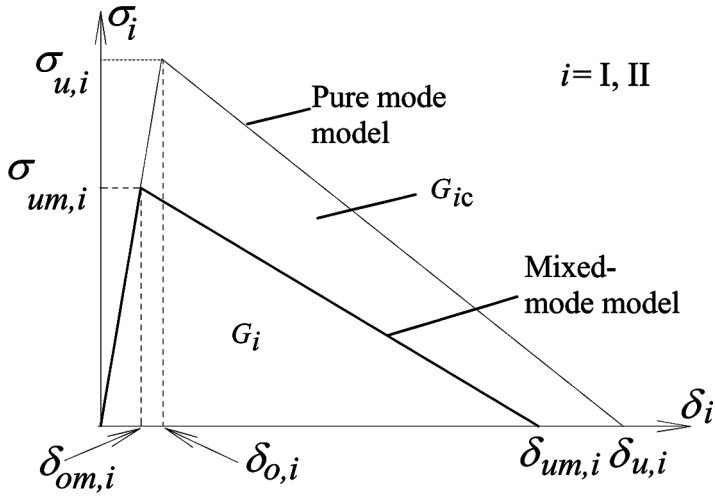

FIGURE 14 Pure and mixed-mode damage model.

ultimate failure, $\delta_{um,i}$, can be obtained from Eqs. (12) and (13), giving the following expressions after some algebraic manipulation detailed elsewhere [17]:

$$\delta_{om,i} = \frac{\beta_i \delta_{om}}{\sqrt{1+\beta_{\mathrm{II}}^2}}, \tag{15}$$

$$\delta_{um,i} = \frac{\beta_i \delta_{um}}{\sqrt{1+\beta_{\mathrm{II}}^2}}, \tag{16}$$

where β_i represent the mode ratios

$$\beta_i = \frac{\delta_i}{\delta_{\mathrm{I}}} \tag{17}$$

and δ_{om}, δ_{um} are the equivalent mixed-mode relative displacements

$$\delta_{om} = \delta_{o,\mathrm{I}}\delta_{o,\mathrm{II}}\sqrt{\frac{1+\beta_{\mathrm{II}}^2}{\delta_{o,\mathrm{II}}^2+\beta_{\mathrm{II}}^2\delta_{o,\mathrm{I}}^2}}, \tag{18}$$

$$\delta_{um} = \frac{1+\beta_{\mathrm{II}}^2}{\delta_{om}\left[(\delta_{o,\mathrm{I}}\delta_{u,\mathrm{I}})^{-1}+\beta_{\mathrm{II}}^2(\delta_{o,\mathrm{II}}\delta_{u,\mathrm{II}})^{-1}\right]}. \tag{19}$$

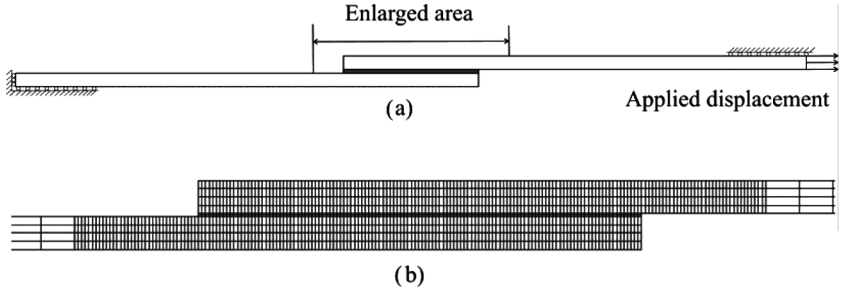

FIGURE 15 Finite element model: a) boundary conditions and b) finite element mesh detail for 0.2-mm adhesive thickness.

The damage parameter can now be obtained by substituting Eqs. (15) and (16) in Eq. (10).

As already mentioned, the failure occurred cohesively close to the adherend–adhesive interfaces. Consequently, the interface elements were placed at adherend–adhesive interfaces, and the properties of the adhesive were considered in the damage model. A very refined mesh was considered in the overlap region to simulate accurately the damage initiation and growth (see Fig. 15). The plane elements simulating the adhesive behaviour had a length of 0.2 mm and a thickness of 0.1 mm. The numerical analysis was performed considering applied displacement, geometric nonlinearity, and an elastoplastic material model for the adhesive. The adhesive plasticity included in the continuum elements and the interface elements were both active. Therefore, the fracture energy of the adhesive will be greater than its critical strain-energy release rate because the continuum will contribute to energy dissipation. This may lead to unconservative failure predictions. The values of strain-energy release rates were not measured experimentally. Typical values for the three adhesives were considered (see Table 3). It should be emphasized that, in this model, the failure loads are mainly dictated by the limiting stress. The critical

TABLE 3 Adhesive Strain-Energy Release Rates (Typical Values)

Parameter	AV138/HV998	Hysol EA 9321	Hysol EA 9361
G_{Ic} (N/mm)	0.3[a]	0.45[b]	2.61[c]
G_{IIc} (N/mm)	0.6	0.9	5.22

[a]Ref. [18].
[b,c]Ref. [19].

strain-energy release rates play their part especially on the postpeak behaviour of the load-displacement curve [20].

The plastic behaviour of the adhesive was modelled using the exponent Drucker–Prager criterion [21], which takes into account the hydrostatic stress. There are other models that include the first stress invariant such as the one of Raghava [22] and the one of Dolev and Ishai [23]. The Raghava and the exponent Drucker–Prager criteria are equivalent when the exponent parameter (b) is 2. The yield criterion can be expressed as

$$aq^b - p = p_t \tag{20}$$

The terms that appear in Eq. (20) are defined as

$$a = \frac{1}{3(\lambda - 1)\sigma_{yt}},$$
$$q = \sqrt{\frac{1}{2}[(\sigma_1 - \sigma_2)^2 + (\sigma_2 - \sigma_3)^2 + (\sigma_3 - \sigma_1)^2]} = \sqrt{3J_2},$$
$$b = 2,$$
$$p = -\frac{1}{3}(\sigma_1 + \sigma_2 + \sigma_3) = -\frac{1}{3}I_1,$$
$$p_t = \frac{\lambda\sigma_{yt}}{3(\lambda - 1)},$$

where λ is the ratio of yield stress in compression to the yield stress in tension, σ_i ($i = 1, 2, 3$) are the principal stresses, σ_{yt} is the yield stress in tension, J_2 is the second deviatoric stress invariant, and I_1 is the first invariant of the stress tensor. Note that when $\lambda = 1$, the exponent Drucker–Prager model is equivalent to the von Mises criterion. Compression tests (ASTM D695-68T) were carried out to determine λ (see Table 4). To illustrate the importance of the hydrostatic stress on the yield, the von Mises and the exponent Drucker–Prager models were represented in a p–q plane as shown in Fig. 16; the horizontal axis (p) corresponds to the hydrostatic axis and the vertical axis (q) represents the deviatoric stress. The plot is for the ductile adhesive (Hysol EA 9361). The experimental data points obtained in tension, in

TABLE 4 Adhesives Ratio of Yield Stress in Compression to Yield Stress in Tension (λ) (Measured Experimentally)

Parameter	AV138/HV998	Hysol EA 9321	Hysol EA 9361
λ	1.3	1.6	1.8

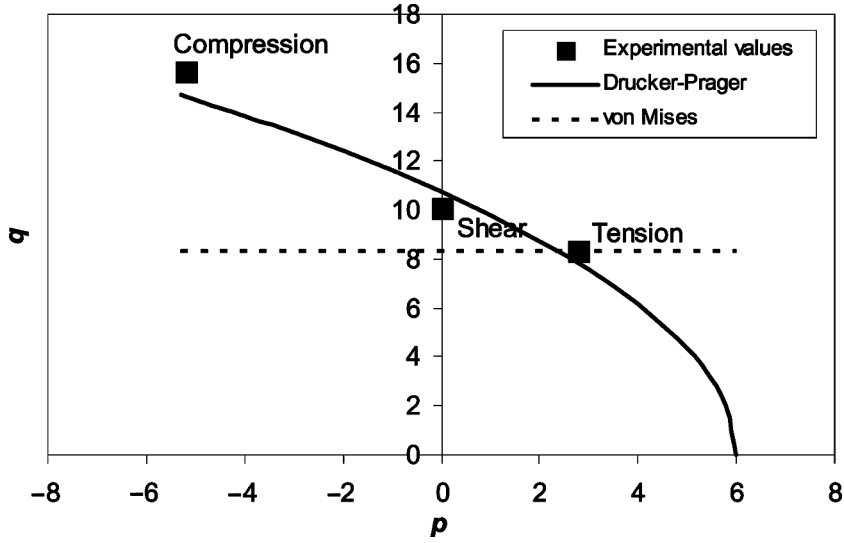

FIGURE 16 Plot of yield models and yield stresses at an effective plastic strain of 0.015 for the ductile adhesive (Hysol EA 9361) on the p–q plane.

compression, and in shear (notched-plate shear method) are also represented, and these lie close to the exponent Drucker–Prager model given by Eq. (20). Figure 16 shows that the von Mises criterion overestimates the yield when there is a high hydrostatic component and these stresses are present in adhesive joints. Various studies have proven [12,24] that the mechanical behaviour of adhesives is better simulated when the hydrostatic stress component is included, especially if the adhesive is very ductile.

4.2. Results

The predicted failure loads are reasonably close to the experimental values, especially for the brittle and intermediate adhesives. Table 5 compares the experimental and the predicted failure loads using the Drucker–Prager model and the interface elements. The predicted failure loads show that the thinner the bondline, the stronger the joint, even for the brittle adhesive (AV138/HV998). This theoretical result indicates that a failure criterion located at the interface gives good predictions and can explain the influence of the adhesive thickness, even though the fracture properties (G_{Ic} and G_{IIc}) introduced in the interface elements were not experimentally measured. The failed

TABLE 5 Comparison of the Experimental and Predicted Failure Loads

Adhesive	Glueline thickness (mm)	Experimental failure load (kN)	Predicted failure load (kN)	
AV138/HV998	0.2	9.6	13.4	
	0.5	9.8	10.8	
	1	8.1	8.1	
Hysol EA 9321	0.2	11.1	11.6	
	0.5	9.5	10.4	
	1	8.2	8.8	
Hysol EA 9361	0.2	12.5	5.2	(11.6[a])
	0.5	11	5.1	(11.3[a])
	1	10	4.9	(10.6[a])

[a]Using properties of adhesive determined for a test speed of 100 mm/min.

joints all had a cohesive failure very close to the interface (see Fig. 7). Note that the predicted failure loads for the ductile adhesive are much lower than the experimental values. This is because the tensile stress–strain values used for the failure load prediction were obtained at a strain rate much lower than the strain rate of the adhesive when tested in a joint. The same crosshead speed was used in both cases (1 mm/min), but for the bulk specimen this corresponds to a strain rate of approximately 0.02/min whereas for the SLJs, the strain rate varies from 1/min (1-mm glueline) to 5/min (0.2-mm glueline). Additional tests were carried out to confirm the viscoelastic nature of the adhesive Hysol EA 9361. Bulk specimens were tested at a crosshead speed of 100 mm/min, which corresponds to a strain rate (approximately 2/min) comparable with the strain rate of the SLJs. Figure 17 shows the stress–strain curves for 1 mm/min and 100 mm/min of Hysol EA 9361 for comparison purposes. The tensile strength goes from 8 (at 1 mm/min) to 22 MPa (at 100 mm/min). With the properties obtained for 100 mm/min, the finite element analysis gave failure load predictions much closer to the experimental values (see Table 5). If the adhesive is relatively brittle and is at a temperature well below its glass-transition temperature (T_g), then it is not very sensitive to strain-rate effects. However, if the adhesive is relatively close to its T_g, which is the case of the ductile adhesive, the material will be viscoelastic and very sensitive to strain-rate effects [25].

The numerical load-displacement curves of the ductile adhesive (see Fig. 18) follow the same pattern as those obtained experimentally (see Fig. 13). Note that the numerical and experimental displacements are not comparable because the experimental displacement corresponds to

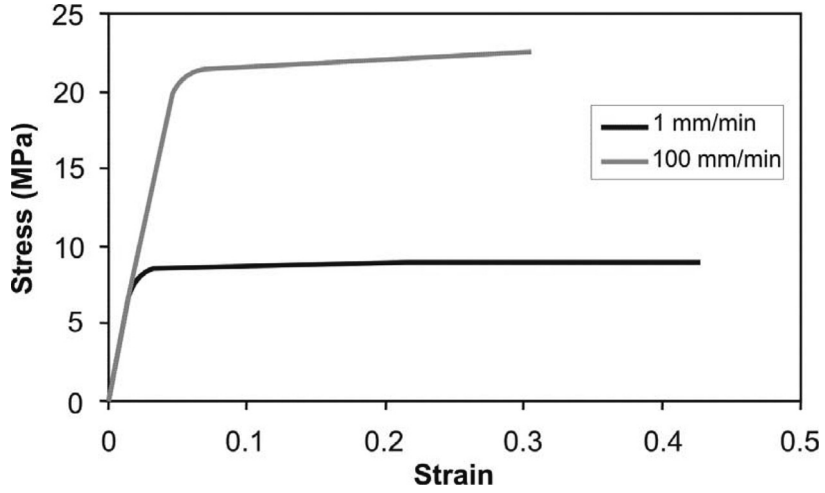

FIGURE 17 Tensile stress–strain curves (bulk specimens) of the ductile adhesive Hysol EA 9361 for 1 mm/min and 100 mm/min cross-head speeds.

the crosshead displacement, which includes the slack and displacement of the loading tool. Based on the change in slope, it can be observed in Fig. 18 that the thinner joint started to deform plastically

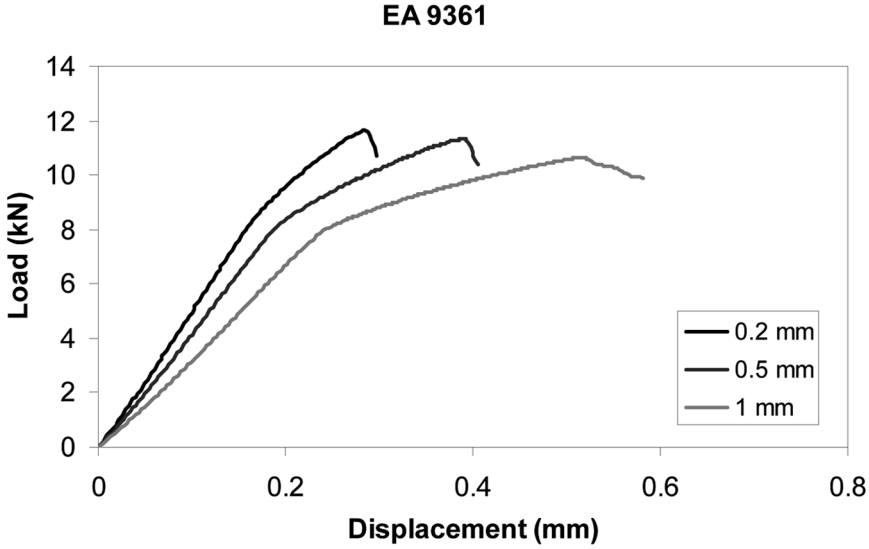

FIGURE 18 Finite element load-displacement curves for the ductile adhesive Hysol EA 9361.

at a higher load than the thicker one. However, it was verified that the localized plastic initiation of the adhesive that occurs at the ends of the overlap does not correspond to a change in slope, which is induced by more extensive plastification. The localized plastic initiation starts at a lower loading displacement and follows Crocombe's [5] predictions (*i.e.*, the thinner the bondline the lower the plastic loading displacement).

5. STATISTICAL ANALYSIS

The experimental plan shown in Table 2, based on the Taguchi method, permits one to assess the influence of the adhesive thickness and the type of adhesive (toughness, U_T) on the lap shear strength. The analysis of variance (ANOVA) (see Table 6) of the experimental results gives the relative importance of these two variables as well as their interaction. The effect of the adhesive thickness is slightly more important than the type of adhesive. The main effect of the adhesive thickness is shown in Fig. 19. It is practically linear. To account for the effect of the type of adhesive, it was decided to use its toughness determined by the area under the stress–strain curve (see Table 1). This quantity best describes the type of adhesive because it includes the effect of the strength as well as the ductility. The main effect of U_T on the failure load is shown in Fig. 20. The relation is also very close to linearity. Note that the correlation obtained between the bulk adhesive toughness and the lap shear strength is valid only for the test conditions used here.

Both effects (adhesive thickness and toughness) were included in the prediction of the failure load according to Eq. (21) [26]:

$$FL_{predict} = M + (\overline{t_{ai}} - M) + (\overline{U_{Ti}} - M), \tag{21}$$

where $FL_{predict}$ is the failure load prediction, M is the average failure load, $\overline{t_{ai}}$ is the effect of the adhesive thickness at the level i, and $\overline{U_{Ti}}$ is the effect of the type of adhesive (toughness, U_T) at level i. The

TABLE 6 Analysis of Variance (ANOVA)

Source	Mean square	F value	P value
Adhesive thickness (mm)	23.191	35.346	0.0001
Type of adhesive	21.456	32.701	0.0001
Interaction (adhesive thickness × type of adhesive)	1.875	2.858	0.0341
Residual	0.656		

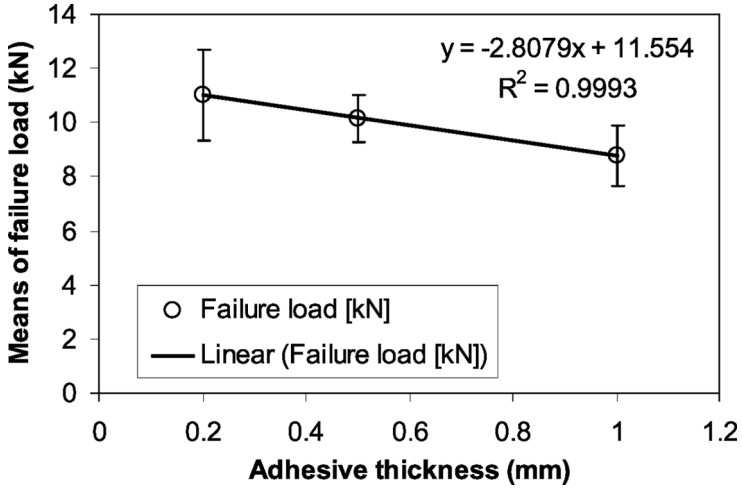

FIGURE 19 Average response graph with 95% error bars for the main effect of adhesive thickness.

interaction (adhesive type × adhesive thickness) was not included in Eq. (21) because the corresponding mean square (1.875, see Table 6) is small in comparison with the effect of adhesive type and adhesive thickness. Note, however, that the interaction effect is statistically

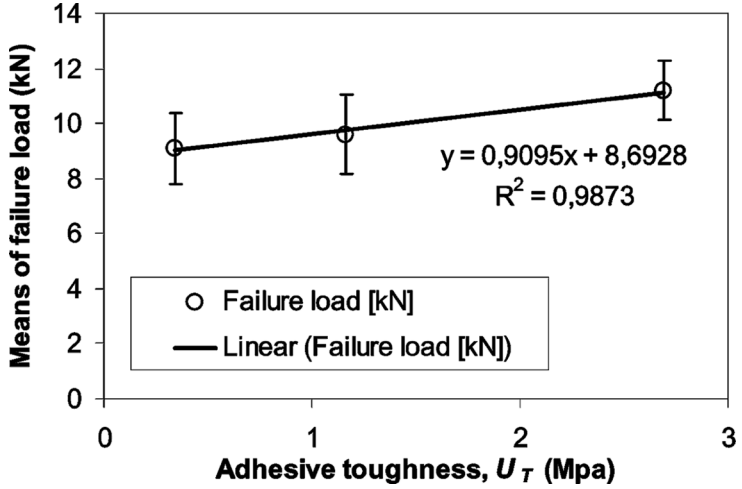

FIGURE 20 Average response graph with 95% error bars for the main effect of the type of adhesive.

TABLE 7 Experimental Validation of the Statistical Failure-Load Prediction

Adhesive	Adhesive thickness (mm)	U_T (MPa)	Predicted failure load (kN)	Experimental failure load (kN)
Araldite 2011	1	5.62	12.59	11.65
Araldite 2011	0.5	5.62	13.99	13.96
Araldite 2011	0.2	5.62	14.83	13.40
Redux 326	0.12	0.75	10.63	10.43

valid for a level of significance of 95% because the P value is lower than 5% (0.0341; see Table 6). The values of $\overline{t_{ai}}$ and $\overline{U_{Ti}}$ can be determined by the equation that best fits the points corresponding to the failure load *vs.* adhesive thickness (see Fig. 19) and the failure load *vs.* adhesive toughness (see Fig. 20), respectively. By doing so, the following expression is obtained:

$$FL_{predict} = 10.28 - 2.81t_a + 0.91U_T, \tag{22}$$

where t_a is the adhesive thickness and U_T is the adhesive toughness. Additional tests were carried out to validate this equation with another adhesive (Araldite 2011 from Huntsman). Tensile tests (1 mm/min) on dogbone specimens ($\sigma_y = 24.5\,\text{MPa}, \sigma_r = 31.7\,\text{MPa}$, and $\varepsilon_f = 0.20$) gave a toughness (U_T) of 5.62 MPa. Table 7 shows that the predicted failure loads using Eq. (22) compare well with the experimental failure loads (1 mm/min). Adhesive Araldite 2011 has the best combination of strength and ductility (*i.e.*, the highest toughness), giving the highest lap shear strength. Equation (22) also gives good predictions for the case of a brittle adhesive (Redux 326 from Hexcel Composite, Stanford, CT, USA) with a bondline thickness not within the range that was used for the statistical analysis. Table 7 shows that the predicted failure load of an SLJ with adhesive Redux 326 is close to the experimental value. The lap shear tests with Redux 326 were obtained in a previous study by one of the authors [10]. Note that when the adherends change or the overlap length is not 25 mm, Eq. (22) is not valid. A larger Taguchi matrix would be necessary to take into account these variables. However, this method shows that a statistical analysis can be an alternative method for the prediction of joint strength.

6. CONCLUSIONS

The effect of adhesive thickness and toughness on the lap shear strength was investigated in this study. The overlap was 25 mm, and the adherends were 2-mm-thick hard steel. The experimental failure

loads were predicted by a finite element analysis considering interface finite elements and incorporating a progressive damage model. The experimental results were statistically treated to give a failure-load predictive equation. The following conclusions can be drawn:

1. The lap shear strength increases as the adhesive thickness decreases.
2. The lap shear strength increases with the adhesive toughness (U_T).
3. The Taguchi method is a valid technique for prediction of lap shear strength.
4. The effect of adhesive thickness on the lap shear strength can be explained by adhesive–adherend interface stresses.
5. The interface elements, including a progressive damage model, are a promising method for the failure load prediction.
6. When predicting the joint failure load with the finite element method, it is important to use the bulk adhesive properties determined for a strain rate similar to the strain rate experienced by the adhesive in the joint.

REFERENCES

[1] Petrie, E. M., *Handbook of Adhesives and Sealants* (McGraw-Hill, New York, 2000), Chap. 4, pp. 151–156.
[2] Lee, D. B., Ikeda, T., Miyazaki, N., and Choi, N. S., *Journal of Engineering Materials and Technology—Transactions of the ASME* **126**, 14–18 (2004).
[3] Volkersen, O., *Luftfahrtforschung* **15**, 41–47 (1938).
[4] Goland, M. and Reissner, E., *J. Appl. Mech.* **66**, A17–A27 (1944).
[5] Crocombe, A. D., *Int. J. Adhes. Adhes.* **9**, 145–153 (1989).
[6] Gleich, D. M., van Tooren, M. J. L., and Beukers, A., *J. Adhes. Sci. Technol.* **15**, 1091–1101 (2001).
[7] Adams, R. D. and Peppiatt, N. A., *J. Strain Anal.* **9**, 185–196 (1974).
[8] Taguchi, G., Chowdhury, S., and Taguchi, S., *Robust Engineering* (McGraw-Hill, New York, 2000).
[9] NF T 76-142, Méthode de préparation de plaques d'adhésifs structuraux pour la réalisation d'éprouvettes d'essai de caractérisation, 1988.
[10] Da Silva, L. F. M., Adams, R. D., and Gibbs, M., *Int. J. Adhes. Adhes.* **24**, 69–83 (2004).
[11] Chousal, J. A. and Gomes, J. F., *Proceedings of M2D, Third International Conference on Mechanics and Materials in Design*, S. A. Meguid (Ed.) (University of Toronto, 2000), pp. 269–270.
[12] Da Silva, L. F. M. and Adams, R. D., *J. Adhes. Sci. Technol.* **29**, 109–142 (2005).
[13] Dieter, G. E., *Mechanical Metallurgy SI Metric Edition* (McGraw-Hill, London, 1988), pp. 282–283.
[14] Taguchi, G. and Konishi, S., *Orthogonal Arrays and Linear Graphs* (Asi Press, Dearborn, MI, 1987), p. 36.

[15] Adams, R. D. and Davies, R., Strength of lap shear joints, in *The Mechanics of Adhesion*, D. A. Dillard and A. V. Pocius (Eds.) (Elsevier, Amsterdam, 2002), pp. 111–144.
[16] Gonçalves, J. P. M., de Moura, M. F. S. F., Magalhães, A. G., and de Castro, P. M. S. T., *Fatigue Fract. Eng. Mater. Struct.* **26**, 479–486 (2002).
[17] De Moura, M. F. S. F., Daniaud, R., and Magalhães, A. G., Simulation of mechanical behaviour of composite bonded joints containing strip defects, *Int. J. Adhes. Adhes. 26*, 464–473 (2006).
[18] Fernlund, G. and Spelt, J. K., *Int. J. Adhes. Adhes.* **11**, 221–227 (1991).
[19] Tomczyk, A. J., MTS Adhesives Project 2: Report no. 5: Summary report: Test methods for adhesive fracture properties, AEAT-0125 (AEA Technology, Oxfordshire, 1997).
[20] Boström, L., Method for determination of the softening behaviour of wood and the applicability of a nonlinear fracture mechanics model, Ph.D. thesis, Srend Institute of Technology, Report TVBM-1012, Lund, Sweden (1992).
[21] Drucker, D. C. and Prager, W., *Quart. Appl. Math.* **10**, 157–165 (1952).
[22] Raghava, R. S., Cadell, R., and Yeh, G. S. Y., *J. Mater. Sci.* **8**, 225–232 (1973).
[23] Dolev, G. and Ishai, O., *J. Adhesion* **12**, 283–294 (1981).
[24] Dean, G., Crocker, L., Read, B., and Wright, L., *Int. J. Adhes. Adhes.* **24**, 295–306 (2004).
[25] Ward, I. M., *Mechanical Properties of Solid Polymers* (John Wiley & Sons, Chichester, UK, 1979), Chap. 12, pp. 368–370.
[26] Fowlkes, W. Y. and Creveling, C. M., *Engineering Methods for Robust Product Design* (Addison-Wesley, Reading, MA, 1995), Chap. 7, pp. 134–136.